Article

Solid Phase Synthesis, DFT Calculations, Molecular Docking, and Biological Studies of Symmetrical N_2,N_4,N_6-Trisubstituted-1,3,5-triazines

Wajiha Akbar, Shahana Ehsan, Sabir Ali Siddique,* Muhammad Sarfraz, Faiqa Shaheen, Ayesha Shafqat, Shahnaz,* Muhammad Bilal Ahmed Siddique, Ayesha Saeed, Rashad Al-Salahi, and Youness El Bakri
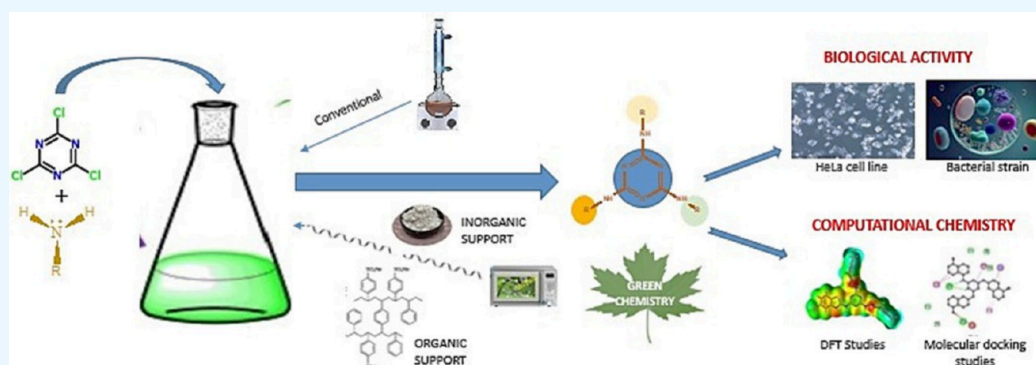
Read Online

ACCESS | Metrics & More | Article Recommendations | Supporting Information

ABSTRACT: A diversity-oriented, multicomponent convergent synthesis of symmetrical triazines through a one-pot protocol is presented in this research project. The assembly of trisubstituted triazines was initially carried out using easily available reagents through three different protocols, i.e., conventional, MW-assisted synthesis, and solid-supported MW-assisted synthesis using organic and inorganic support to carry out a comparative analysis as to which procedure best corresponds to a greener synthesis protocol. The compounds formed were characterized for structure elucidation and subjected to *in vitro* anticancer and antibacterial screening. Additionally, computational studies, such as DFT calculations and molecular docking analyses, were conducted.

1. INTRODUCTION

In today's rapidly progressing world, increasing pollution and health issues are a major concern, resulting from numerous scientific developments that, while impressive, have often led to significant challenges for humanity's peace of mind and body.

Moreover, this distressing situation has been intensified by the current occurrence of drug resistance and deadly infections. Therefore, all energy has been focused on the prompt synthesis of new compatible drugs possessing a promising potential to fight fatal diseases. This has indeed stimulated the synthetic chemists to come up with novel means of drug formation with manifold potentials.[1,2]

Nitrogen containing heterocyclic compounds are essential building blocks of numerous natural products, pharmaceuticals and organic/polymeric materials.[3] In particular, triazines present one of the most important frameworks among heterocyclic systems. Not only have they emerged as important intermediates in synthetic organic chemistry but also they possess medicinal significance due to numerous bioactivities associated with them.

The structure of triazine is based on a planar six-membered heterocyclic ring resembling that of a benzene ring, except that three carbon−hydrogen units of benzene are replaced with nitrogen−hydrogen units. Triazine occurs in three isomeric forms (Figure 1) due to the distinguished position of nitrogen atoms in the ring system, i.e., 1,2,3-vicinal triazine, 1,2,4-isotriazine (asymmetrical triazine), and 1,3,5-s-triazine (cyanidine).[4,5]

Among these, s-triazine is commonly used in organic reactions due to its unique configuration and biological properties. Its structural similarity to naturally occurring heteroaromatic compounds like nucleotides and nucleosides allows it to generate biophores with significant therapeutic potential, fighting diseases such as leukemia, malaria, tuberculosis, diabetes, HIV, etc. Moreover, they also display
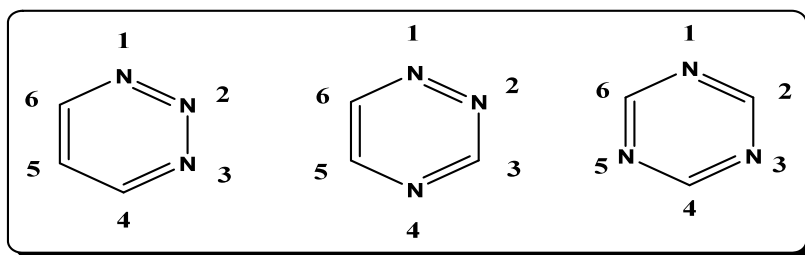
Figure 1. Isomeric forms of triazine.

remarkable resistance against microbes such as bacteria, virus, and fungus and are potent anti-inflammatory agents as well.[6,7]

s-Triazines that have substituents like triethylamine, morpholine, or a benziimidazole ring exhibit excellent inhibition against cancer cell lines and are used in many clinically approved drugs, as well as Dioxadet, Decitabine, metformin, etc.[8]

The eminent reactivity and extensive applicability of the triazine core fragment is attributed to its weakly basic property and comparatively higher electron affinity in contrast to other heteroatoms such as pyrimidine. This is due to the increased polarity of C−N bonds present, resulting from the partial location of the π electrons on the ring nitrogen instead of the delocalization of electrons as is the case of the benzene ring (Figure 2). As a result, triazine acts as a strong electron-withdrawing scaffold and readily undergoes nucleophilic substitution reactions.[9,10]
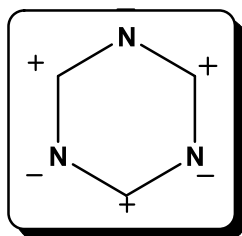

Figure 2. Electron system in triazine.

Moreover, s-triazines have good synthetic accessibility from TCT (cyanuric chloride), where all three chlorine atoms possess varied levels of reactivity and can be replaced selectively according to the conditions provided. The first chlorine atom readily undergoes substitution at 0 °C in the presence of a nucleophile, while the second substitution occurs around 35 °C and the third substitution requires comparatively higher temperatures of 80−100 °C, leading to the formation of mono-, di-, and trisubstituted triazines. This allows the manipulation of the derived triazine compounds with multiple functionalities of different nature and plays a vital role in fashioning these promising scaffolds of diverse pharmacological characteristics.[11,12]

Thus, cyanuric chloride derived triazines are imperative synthetic targets, and their efficacy as a multipurpose moiety gives them a headstand in the discipline of organic synthesis. However, symmetrical triazines comprising active functional groups derived from cyanuric chloride have not been subjected to active research in the past due to the complications faced while synthesizing them. Nevertheless, the scope encompassed by these complicated, yet enormously worthy compounds call

for an additional and thorough study to be done in those areas, too, where previously no success has been achieved.[13]

Therefore, we report herein the synthesis, biological evaluation, and computational studies, such as DFT and molecular docking of symmetrical triazines.
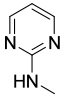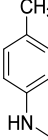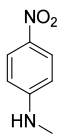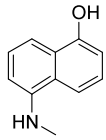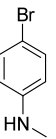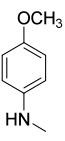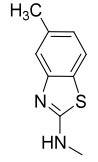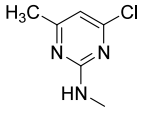
2. EXPERIMENTAL SECTION

2.1. Chemistry. The chemicals employed in the reactions were of analytical grade from Sigma-Aldrich. MW DW-180, 2450 MHz, and 950 W were used for microwave-assisted methodologies. The Gallenkamp mp apparatus was used for determining the melting points. Midac FT-IR spectrophotometer (M2000) was used for FT-IR spectroscopy in the range of 400−4000 cm^{-1} using a KBr disc. MS was performed using a JEOL JMS 600H-1 spectrometer by direct probe. ^{1}H and ^{13}C NMR were done on Bruker AVANCE III NMR spectrometers at 500 and 151 MHz, respectively. See Table 1 for a compiled list of synthesized compounds.

2.1.1. General Procedure for the Synthesis of Symmetrical Triazines via a Classical Approach. Cyanuric chloride (0.1845 g/0.1 mmol) was first dissolved in 1,4-dioxane (5.0 mL). To this, substituted amine (0.3 mmol) was added and refluxed for 6 h (Scheme 1). The progress of the reaction was observed using TLC (ethanol/n-hexane, 8:2) at regular intervals. After completion of the reaction, workup was performed using ice-cold distilled water. The precipitates that were formed as a result were first filtered, then washed, and afterward recrystallized using ethanol to get a pure product.

2.1.2. General Procedure for the Synthesis of Symmetrical Triazines via Microwave-Assisted Methodology. Initially, cyanuric chloride (0.1845 g/0.1 mmol) was dissolved in 1,4-dioxane (5.0 mL). To it, substituted amine (0.3 mmol) was added and then irradiated with microwaves. After the reaction had been completed as indicated by TLC (ethanol/n-hexane, 8:2), ice-cold distilled water was added resulting in the formation of precipitates that were first filtered then washed, and afterward recrystallized using ethanol to get pure product.[14]

2.1.3. General Procedure for the Synthesis of Symmetrical Triazines via Solid-Supported Microwave-Assisted Synthesis Using Celite (Inorganic Support). Initially, a mixture of cyanuric chloride (0.1845 g/0.1 mmol) in 1,4-dioxane (3.0 mL) was adsorbed on an inorganic solid support (Celite 1 g). Then, substituted amine (0.3 mmol) was added to it, and the reaction mixture was irradiated with microwaves at an interval of 5 s each. After the reaction had been completed as indicated by TLC (ethanol/n-hexane, 8:2), a workup was carried out using ice-cold distilled water. The precipitates thus formed along with the solid support were filtered and then dissolved in ethanol, whereby the insoluble solid support was separated by

Table 1. Structural Formula, Reaction Time, and Percentage Yield of the Synthesized Compounds

Compd.	Substituent R	Conventional		MW-Assisted		MW-Assisted Solid-supported			
						Organic support		Inorganic support	
		Reaction time	% yield	Reaction time	% yield	Reaction time	% yield	Reaction time	% yield
S1		6 h	76%	2 min 50 sec	87%	1 min 5 sec	93%	1 min 40 sec	90%
S2		6 h	78%	2 min 55 sec	86%	55 sec	94%	1 min 10 sec	90%
S3		6 h	77%	2 min 40 sec	86%	50 sec	93%	1 min 15 sec	89%
S4		6 h	74%	3 min	85%	50 sec	92%	1 min 10 sec	88%
S5		6 h	73%	2 min 40 sec	84%	60 sec	92%	1 min 20 sec	87%
S6		6 h	76%	2 min 30 sec	86%	1 min 10 sec	95%	1 min 35 sec	92%
S7		6 h	68%	2 min 55 sec	79%	1 min 15 sec	94%	1 min 40 sec	88%
S8		6 h	66%	2 min 40 sec	79%	60 sec	91%	1 min 20 sec	86%

filtration and the product was recrystallized to enhance its purity.

2.1.4. General Procedure for the Synthesis of Symmetrical Triazines via Solid-Supported Microwave-Assisted Synthesis Using Cross-Linked Sodium Polystyrenesulfonate (Organic Support). Initially, a mixture of cyanuric chloride (0.1845 g/ 0.1 mmol) in 1,4-dioxane (3.0 mL) was mixed with polymer-based organic solid support (cross-linked sodium polystyrenesulfonate, 1 g) and irradiated for 40 s. Then, substituted amines (0.3 mmol) were added and irradiated with microwaves

Scheme 1. Scheme of Synthesis of Triazine
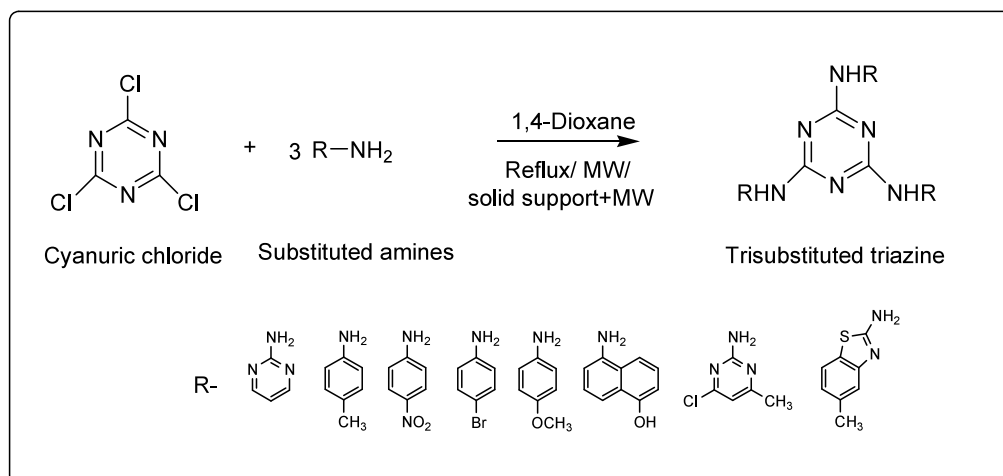
at an interval of 5 s each. After the reaction had been completed as indicated by TLC (ethanol/*n*-hexane, 8:2), a workup was carried out using ice-cold distilled water. The precipitates thus formed along with the solid support were filtered and then dissolved in ethanol, whereby the insoluble solid support was separated by filtration, and the product was recrystallized to enhance its purity.

2.1.4.1. N₂,N₄,N₆-Tri(pyrimidin-2-yl)-1,3,5-triazine-2,4,6-triamine S1. Off white solid; yield 91%; mp 222−223; IR (KBr, cm⁻¹): 3400 (NH), 1608.63, (C=C stretch Ar), 3100 (C−H stretch), 1550.77 (N−H bend), 1377.17 (C−N stretch), 775.38 (C−H bend Ar); MS (*m/z*): 360.1 (M⁺), 352.1, 282.1, 225.2, 137.0, 78.1; ¹H NMR (500 MHz, CDCl₃) δ 3.49 (s, 3H), 6.71 (t, *J* = 5.0 Hz, 3H), 8.34 (d, *J* = 4.9 Hz, 6H); ¹³C NMR (126 MHz, CDCl₃) δ 161.56, 158.40, 157.78, 111.42.

2.1.4.2. N₂,N₄,N₆-Tri-p-tolyl-1,3,5-triazine-2,4,6-triamine S2. White solid; yield 94%; mp 183−184; IR (KBr, cm⁻¹): 3337.57 (NH), 1620.21, (C=C stretch Ar), 3167.12 (C−H stretch), 1577.77 (N−H bend), 1400.32 (C−N stretch), 1450.47 (C−H bending methyl), 705.95 (C−H bend Ar); MS (*m/z*) 396 (M⁺), 357, 352, 306, 250, 189, 185, 133, 118, 105, 90; ¹H NMR (500 MHz, CDCl3) δ 8.53 (d, *J* = 2.3 Hz, 6H), 7.58 (d, *J* = 8.9 Hz, 6H), 3.70 (s, 3H), 1.25 (s, 9H); ¹³C NMR (126 MHz, CDCl₃) δ 164.05, 134.83, 132.37, 132.03, 122.78, 67.09.

2.1.4.3. N₂,N₄,N₆-Tris(4-nitrophenyl)-1,3,5-triazine-2,4,6-triamine S3. Light brown solid; yield 93%; mp 203; IR (KBr, cm⁻¹): 3336.85 (NH), 1620.21 (C=C stretch Ar), 3100 (C−H stretch), 1589.34 (N−H bend), 1550.77 (N−O stretch), 1373.74 (C−N stretch), 748.38 (C−H bend Ar); MS (*m/z*): 489.2 (M⁺), 459.2, 443.3, 367.1, 352.2, 206.0, 164.0, 76.0, 44.0; ¹H NMR (500 MHz, CDCl₃) δ 3.71 (s, 3H), 7.45 (d, *J* = 8.9 Hz, 6H), 7.53 (d, *J* = 8.9 Hz, 6H); ¹³C NMR (126 MHz, CDCl₃) δ 164.16, 126.35, 125.24, 120.36, 113.39.

2.1.4.4. N₂,N₄,N₆-Tri(naphthalen-1-ol)-1,3,5-triazine-2,4,6-triamine S4. Brown solid; yield 92%; mp 301; IR (KBr, cm⁻¹): 3400 (OH), 3205 (NH), 1620 (C=C stretch Ar), 2871, 1705 (C=C, C=N), 1558.48 (N−H bend), 1327.32 (O−H bend), 1292.31 (C−N stretch), 705.95 (C−H bend Ar); MS (*m/z*): 552.0 (M⁺), 455.1, 420.0, 378.1, 157.0, 143.0, 127.0, 117.0, 90.0, 84.0, 68.0, 43.0; ¹H NMR (500 MHz, CDCl₃) δ 10.56 (s, 3H), 7.91−7.69 (m, 9H), 7.63−7.45 (m, 9H), 3.69 (s, 3H);

¹³C NMR (126 MHz, CDCl₃) δ 162.00, 161.06, 130.33, 123.25, 122.68, 122.54, 122.10, 115.66.

2.1.4.5. N₂,N₄,N₆-Tris(4-bromophenyl)-1,3,5-triazine-2,4,6-triamine S5. Dark brown solid; yield 92%; mp 268; IR (KBr, cm⁻¹): 3400 (NH), 1604.77, (C=C stretch Ar), 1219.01 (C−N stretch), 1546.91 (N−H bend), 1334.74 (C−N stretch), 775.38 (C−H bend Ar), 621.08 (C−Br); MS (*m/z*) 591.1 (M⁺), 511.2, 431.1, 261.1, 239.1, 195.1, 127.0, 105.1, 78.9, 77.0, 68.0, 52; ¹H NMR (500 MHz, CDCl₃) δ 3.81 (s, 3H), 6.92 (d, *J* = 9.0 Hz, 6H), 7.40 (d, *J* = 9.0 Hz, 6H); ¹³C NMR (126 MHz, CDCl₃) δ 169.56, 131.90, 122.42, 118.76, 117.45.

2.1.4.6. N₂,N₄,N₆-Tris(4-methoxyphenyl)-1,3,5-triazine-2,4,6-triamine S6. White solid; yield 95%; mp 216; IR (KBr, cm⁻¹): 3300 (NH), 1620.21, (C=C stretch Ar), 2900 (C−H stretch), 1573.91 (N−H bend), 1238.30 (C−O stretch), 1307.74 (C−N stretch), 771.95 (C−H bend Ar); MS (*m/z*) 444.3 (M⁺), 429.3, 322.1, 280.1, 266.1, 253.1, 148.1, 122.1, 78.03, 52.0; ¹H NMR (500 MHz, CDCl₃) δ 3.70 (s, 9H), 3.96 (s, 3H), 8.53 (d, *J* = 2.3 Hz, 6H), 7.58 (d, *J* = 8.9 Hz, 6H); ¹³C NMR (126 MHz, CDCl₃) δ 184.92, 168.06, 141.67, 125.40, 99.80, 77.17, 45.79.

2.1.4.7. N₂,N₄,N₆-Tris(5-methylbenzo[d]thiazol-2-yl)-1,3,5-triazine-2,4,6-triamine S7. Light yellow solid; yield 94%; mp 298; IR (KBr, cm⁻¹): 3402.43 (NH), 1620.21, (C=C stretch Ar), 2904.80 (C−H stretch), 1234.44 (C−N stretch), 1581.63 (N−H bend), 1469.76 (C−H bending methyl), 806.255 (C−H bend Ar); MS (*m/z*) 567.1(M⁺), 525.0, 504.3, 405.1, 273.1, 243.0, 164.1, 148.1; ¹H NMR (500 MHz, CDCl₃) δ 1.23 (s, 9H), 3.75 (s, 3H), 7.05 (s, 3H), 8.54 (d, *J* = 2.3 Hz, 3H), 7.59 (d, *J* = 9.1 Hz, 3H); ¹³C NMR (126 MHz, CDCl₃) δ 162.00, 161.06, 137.16, 130.33, 128.14, 122.13, 114.77, 111.24, 45.85.

2.1.4.8. N₂,N₄,N₆-Tris(4-chloro-6-methylpyrimidin-2-yl)-1,3,5-triazine-2,4,6-triamine S8. Yellow solid; yield 91%; mp 282; IR (KBr, cm⁻¹): 3336.85 (NH), 1681.93 (C=C stretch Ar), 3155.54 (C−H stretch), 1261.44 (C−N stretch), 1543.05 (N−H bend), 1485.19 (C−H bending methyl), 824.53 (C−H bend Ar), 779.24 (C−Cl); MS 505.5 (M + 1), 489.1, 475.0, 460.1, 343.5, 254.1, 168.1, 143.1, 127.1; ¹H NMR (500 MHz, CDCl₃) 2.32 (s, 9H), 5.52 (s, 3H), 6.52 (s, 3H); ¹³C NMR (126 MHz, CDCl₃) δ 169.51, 157.18, 122.41, 118.80, 117.44, 29.69.
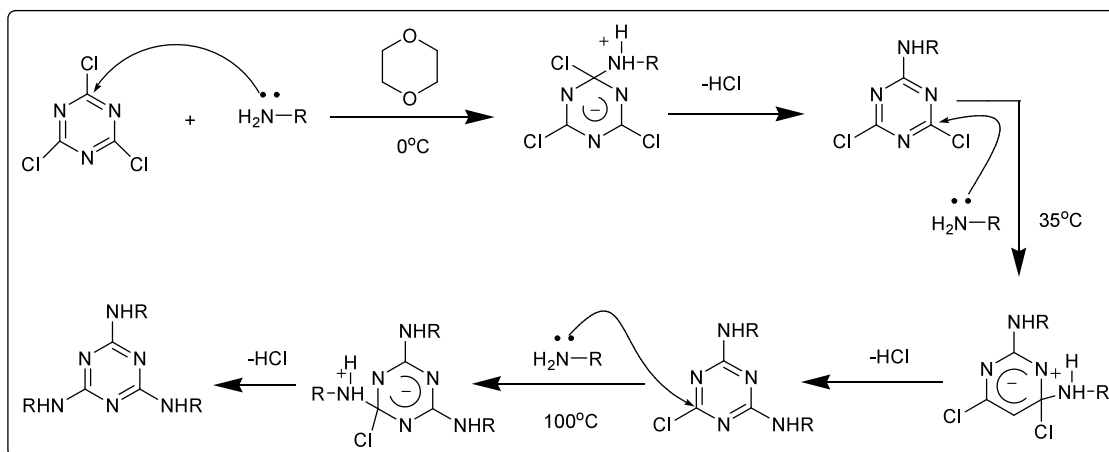
Figure 3. Mechanism of the reaction of cyanuric chloride with substituted amines.
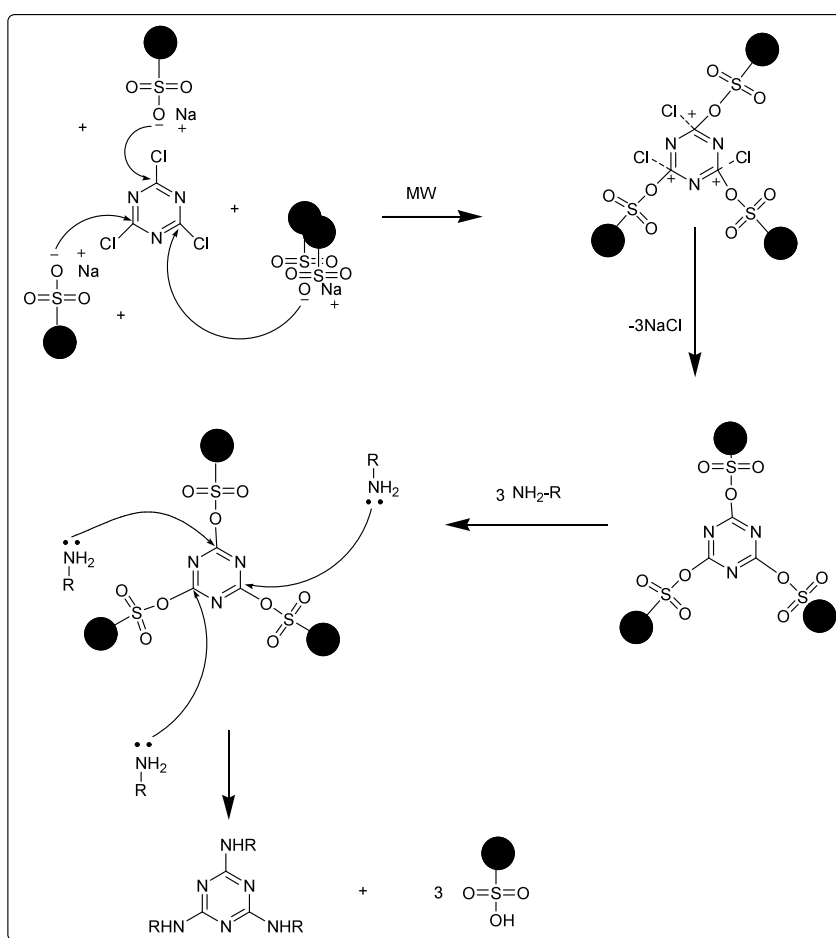
Figure 4. Mechanism of reaction of TCT with nucleophiles in the presence of a polymeric support.

3. RESULT AND DISCUSSION

3.1. Chemistry. Keeping in mind the norms of green chemistry and sustainability, the present organic synthesis was aimed to assemble novel and reported symmetrical trisubstituted triazine derivatives using cyanuric chloride and different amines through different techniques in a one-pot protocol. The synthetic protocol was designed and carried out in such a way that there was conservation of time and energy along with the minimization of the use of hazardous solvents while giving excellent yields of the pure product within a short

period. These were achieved by the use of microwaves instead of the tedious traditional heating system which led to the speedy formation of desired compounds and avoided the formation of side products thus increasing the overall atom economy of the reaction.[15,16]

Along with it, the reactions were carried out on a solid-supported platform that reduced the consumption of solvents and the products formed had a higher degree of purity such that there was no further requirement for tedious purification procedures.[17]

Table 2. Mean of Percentage Cell Viability at Different Concentrations and IC$_{50}$ Values of the Synthesized Compounds

| conc. (μg/mL)	mean of % cell viability							
	S1	S2	S3	S4	S5	S6	S7	S8
control	100	100	100	100	100	100	100	100
DMSO	99.24	99.24	99.24	99.24	99.24	99.24	99.24	99.24
12.5	96.11	97.33	98.59	97.33	82.29	98.59	97.33	97.59
25	78.12	95.24	77.59	75.24	71.98	78.803	79.24	81.87
50	69.29	86.23	70.58	69.54	69.28	71.21	69.54	77.44
100	61.04	78.43	66.99	62.22	56.29	64.54	62.22	71.22
200	53.44	69.12	54.99	52.59	50.01	55.51	56.59	59.51
400	46.11	55.33	45.31	43.59	47.29	44.29	45.67	50.02
IC$_{50}$ (μM) $\pm$ SD	2.0145	46.20	1.8514	1.5716	2.162	1.8227	1.7338	4.785
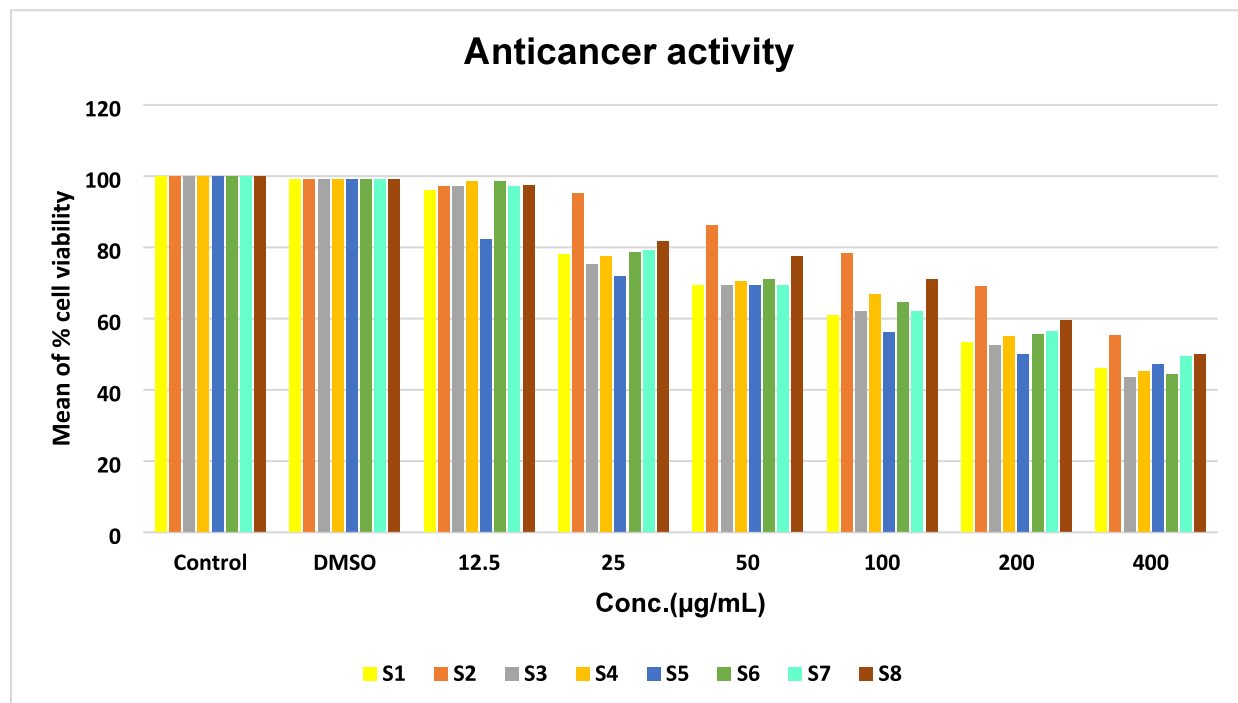
Figure 5. Cytotoxicity graph of MTT assay.

The mechanism of this reaction (Figure 3) depicted the nucleophilic aromatic substitution of all three chlorine atoms of cyanuric chloride by substituted amines through an addition−elimination mechanism. It is also known as S$_N$Ar or Ipso substitution reaction. Substitution of the first chlorine atom occurred readily at low temperatures, but it became comparatively more difficult to achieve second and third chlorine atoms, which was eventually accomplished by gradually raising the temperature up to 100 °C. This is probably because there is a subsequent reduction in the electrophilic character of the carbon attached to the second and third chlorine atom due to the addition of the substituents on triazine because after the chlorine atom is detached from TCT, the electron withdrawal caused by σ-bond is lost. Instead, there is an electronic donation of π-orbital of the added nucleophiles.[18]

The reaction in the presence of polymer support becomes more facilitated as the nucleophilic oxygen of cross-linked sodium polystyrenesulfonate (SPS) containing a partial negative charge attacks the electrophilic carbon of the triazine ring during the application of microwaves, resulting in the elimination of sodium chloride (Figure 4). Then, the lone pair of the nucleophilic amino group of substituted amines attacks these highly electrophilic carbon containing a partial positive charge due to the inductive effect resulting from the highly electron-withdrawing property of the sulfonyl group which tends to make it a good leaving group as well. Moreover, the attack is also facilitated by the resonance stabilized structures of the polymer phenyl ring. As a result, the polymeric solid support easily detaches itself and results in the formation of trisubstituted triazine in a comparatively shorter period with an enhanced yield.

The products formed were structurally elucidated using FTIR, MS, ^{1}H NMR, and ^{13}C NMR techniques and were also biologically tested to check their medicinal efficacy against tumors and microbes such as bacteria and fungus.

3.2. Biological Activity. *3.2.1. Anticancer Activity.* The anticancer activity was determined using the MTT assay. It is an in vitro assay that directly gives an estimate of the percentage of viable cells after they have been exposed to the anticancer compound under consideration. In this activity, a 96-well plate was used containing the HeLa cell line that was treated with different concentrations of synthesized compounds, along with a control containing no drug and simple

Table 3. Zone of Inhibition of the Synthesized Compounds against Gram-Positive and Gram-Negative Bacteria at Different Dilutions

zone of inhibition (mm)		compounds							
		S1	S2	S3	S4	S5	S6	S7	S8
Gram-positive bacteria (*S. aureus*)	50 (mg/mL)	10		17	16	14	16	12	15
	100 (mg/mL)	13		20	19	16	18	15	17
	200 (mg/mL)	17		26	24	21	23	19	21
Gram-negative bacteria (*E. coli*)	50 (mg/mL)	8		16	16	12	17	9	13
	100 (mg/mL)	10		20	19	15	20	10	15
	200 (mg/mL)	13		24	23	18	24	12	18

DMSO. Afterward, MTT was added into these wells, and after a period of 4 h, DMSO was added into the contents of these wells to check absorbance at 570 and 620 nm to measure the amount of purple formazon formed from MTT.[19] Doxorubicin (DOX) was used as the reference drug that had the IC$_{50}$ value of 1.45 ± 0.15.[20]

This activity illustrated that after exposure to different concentrations of the synthesized compounds, the healthy cells underwent cell lysis at different extents owing to the potency of the compound to which they were exposed to. Moreover, the greater the concentration, the greater cell lysis that occurred, resulting in a lower number of viable cells (see Table 2 and Figure 5).

According to the activity carried out, compounds S1, S3, S4, S6, and S7 proved to be the most active compounds among all, while compound S2 showed minimum activity. The rest of the compounds, i.e., S5 and S8, showed moderate activity. These results depicted that the presence of three hydroxyl groups on the phenyl ring around the core s-triazine moiety greatly enhanced its inhibition power as compared to other groups. Moreover, compounds containing methoxy and nitro substituents also showed good activity. Similarly, the presence of the pyridine ring and benzothiazole ring had an enhanced effect on the anticancer activity, while compounds containing methyl substituents showed considerable decrease in activity.

The IC$_{50}$ values also depicted that S3, S4, S6, and S7 were required in the minimum amount among the rest of the compounds to inhibit 50% of the cytotoxic cell.[21,22]

3.2.2. Antibacterial Activity. This activity was carried out using the agar broth dilution method against two bacterial strains, namely, *Staphylococcus aureus* (Gram-positive bacteria) and *E. coli* (Gram-negative bacteria). The synthesized compounds were assessed at three different dilutions, and it was observed that the greater the dilutions were, the lesser was the zone of inhibition. The reference drug used was erythromycin for Gram-positive bacteria and ciprofloxacin for Gram-negative bacteria showing a zone of inhibition of 28 and 25 mm, respectively. Ethanol was used as a control that showed no activity.[23]

Except for compound S2, moderate to good activity was observed against both Gram-positive and Gram-negative bacteria. In the case of both Gram-positive and Gram-negative bacteria, triazines containing nitro phenyl group (S3) showed maximum activity against these bacteria, while compounds substituted with electron-donating groups that had oxygen in them, such as hydroxyl and methoxy groups (S4 and S6), also showed excellent activity. Good inhibition was also observed in compounds (S5) and (S8) that had halogen substitution on them (see Table 3).
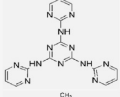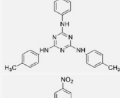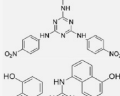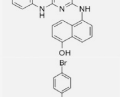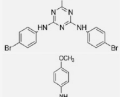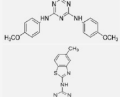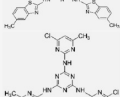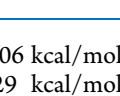
3.3. Molecular Docking Studies. A molecular docking approach was used to study the binding affinities of

synthesized compounds against Receptor Tyrosine Kinases (RTKs), and AutoDockTools program (Version 1.5.7) was used to perform the docking studies.[24] The required 3D protein structures were retrieved from RCSB PDB (https://www.rcsb.org/) which were optimized and prepared before the docking studies.[25] Auto Dock Tool (ADT) was used to remove all water molecules from the protein and any ligands that are attached to these protein structures, followed by energy minimization. The structures of ligands were drawn and then converted into the PDB format using ChemSketch (Version 21) and Open Babel software.[26] The molecular docking studies of active compounds were performed using AutoDockTools version 1.5.7 software. The Grid box was set to cover the active site of the crystal structure with the appropriate dimensions for all receptors. The generated structures were visualized and analyzed through the Discovery Studio 2021 Client version.

3.3.1. Results of Molecular Docking Studies. Targeted therapy is an advanced strategy in cancer treatment that specifically targets certain RTKs in cancer cells as these proteins are involved in stimulating uncontrolled growth and proliferation of cells.[27,28] The combination of growth regulators and chemokines inside the tumor microenvironment triggers complex signaling cascades that propel the advancement of cancer.[29] Compared to conventional chemotherapies, targeted treatments against these substrates including Epidermal Growth Factor Receptor (EGFR), Vascular Endothelial Growth Factor Receptor 2 (VEGFR2), Fibroblast Growth Factor Receptors (FGFRs), Proto-oncogene tyrosine-protein kinase SRC, and Hepatocyte Growth Factor Receptor (HGFR/c-MET) provide more focused and efficient therapy choices by attempting to disrupt signaling pathways that are essential for tumor growth, survival, and metastasis.[30−32] To address the shortcomings of existing treatments, get past resistance mechanisms, target a wider variety of cancer-driving kinases, lessen side effects, and improve treatment efficacy, more research and development of novel TKIs is required. These developments could lead to safer, more individualized, and more effective cancer treatments, which would eventually improve patient outcomes.[33−35] Targeted therapy development is greatly aided by *in silico* studies, which offer insightful information at every step of the process thus accelerating the identification and optimization of drug candidates.[36−38]

Among the screened motifs against the selected target substrates, compounds S1, S4, S6, and S7 were found to be good binders of target proteins. Although the compound S1 had no substituents at the pyrimidine rings but this compound still showed greater binding energies of −12.41, −13.30, −9.77, −8.37, −11.09, and −9.01 kcal/mol with Ligand Efficiency (LE) values of −0.46, −0.48, −0.36, −0.31, −0.41, and −0.33 kcal/mol, respectively, as shown in Table 4. The compound S4 with nitrogen connected to three 1-naphthol moieties with the

Table 4. Ligand–Proteins Binding Energies and Ligand Efficiencies (LE) of the Docked Molecules in the Binding Pockets of Cancer Drug Targets EGFR, VEGFR2, FGFR, SRC, and HGFR

Compounds	Lowest binding energy/Ligand efficiency						Two-dimensional structures
	EGFR 5WB7	EGFR 1M17	VEGFR2 2XIR	FGFR 4QQT	SRC 1YOJ	HGFR 1R0P	
S1	−12.41/−0.46	−13.30/−0.48	−9.77/−0.36	−8.37/−0.31	−11.09/−0.41	−9.01/−0.33	
S2	−8.52/−0.28	−9.86/−0.33	−8.59/−0.29	−7.66/−0.26	−9.73/−0.32	−8.34/−0.28	
S3	−7.14/−0.20	−9.26/−0.26	−9.24/−0.26	−9.68/−0.27	−9.43/−0.26	−9.03/−0.25	
S4	−11.22/−0.27	−12.18/−0.29	−10.84/−0.26	−11.07/−0.26	−12.40/−0.30	−12.06/−0.29	
S5	−7.82/−0.24	−8.77/−0.27	−7.20/−0.22	−7.44/−0.23	−9.07/−0.27	−7.64/−0.23	
S6	−9.11/−0.30	−10.34/−0.34	−8.42/−0.28	−8.42/−0.28	−10.62/−0.35	−9.17/−0.31	
S7	−10.06/−0.26	−11.61/−0.30	−10.98/−0.28	−10.03/−0.26	−11.86/−0.30	−11.72/−0.30	
S8	−8.19/−0.25	−9.26/−0.28	−9.33/−0.28	−8.36/−0.25	−8.89/−0.27	−8.99/−0.27	

best binding energies of −12.18, −12.40, and −12.06 kcal/mol along with the LEs of −0.29, −0.30, and −0.29 kcal/mol against the target substrates EGFR, SRC, and HGFR, respectively. The compound **S6** was found to be potent inhibitor of EGFR and SRC protein whereas the ligand **S7** also showed excellent binding energies of −11.61, −10.98, −11.86, and −11.72 kcal/mol against the EGFR, VEGFR2, SRC, and HGFR target substrates (Table 4).

The ligand–protein binding analysis of compound **S1** with EGFR revealed the importance of carboxylate anions of Glu258 and Glu367 that formed π-anion interactions with two pyrimidine moieties and a triazine ring simultaneously from distances of 2.71, 3.15, and 3.37 Å. A π–σ force (3.80 Å) existed between the third pyrimidine ring of the ligand molecule and Ile370, while the amino acid residues Asn256, Ala329, and Lys333 bound the **S1** through van der Waals forces (3.47, 5.17, and 4.90 Å). The intermolecular interactions between ligand **S4** and the receptor molecule were greater in quantities and were stronger in which the hydroxyl groups present at para positions constituted conventional hydrogen bonding (3.34 and 3.26 Å) with Arg817 and Lys851 amino acid residues while a nitrogen atom of the triazine ring was forming a conventional hydrogen bond (2.15 Å) with the terminal ammonium moiety of Lys721. Additionally, the three naphthyl ring systems were hub of electronic clouds as suitable moieties for constituting π-anion and π-cation forces of attraction with neighboring amino acid residues including Lys721 (4.96 Å), Glu734 (4.48 and 4.50 Å), Asp813 (3.55 and 4.75), Arg817 (3.92 Å), and Asp831 (3.10, 3.52, and 3.93 Å)

while a π-lone pair interaction (2.56 Å) was formed with the Asp831. The aromatic ring of Phe699 was involved in constituting two π–π stacked forces with the nitrogen substituted ring of naphthyl moiety (5.24 Å) and the central triazine ring (5.70 Å) of the ligand molecule. The π-anion forces were found to be the key binding strings to hold compound **S7** in the binding pocket of the VEGFR2 macromolecule where the amino acid Asp1046 was engaged with the triazine ring (4.42 Å) and the carboxylate anion of Glu885 with the five and six membered ring of one of the 5-methylbenzothiazole moiety (2.94 and 3.42 Å). Another important type of forces binding all of the benzothiazole systems of the ligand molecule were π–σ forces of attraction with the Lys A:868 (3.86 Å), Leu A:882 (3.70 Å), Leu A:889 (3.87 Å), Asp A:1028 (3.93 Å), and Leu A:1049 (3.10 and 3.58 Å). The rest of the amino acid residues, including Leu A:870, Ala A:881, Leu A:882, Ile A:892, Val A:898, Leu A:1019, Arg A:1027, Ile A:1044, Leu A:1049, Tyr A:1059, Leu A:1067, and Pro A:1068, in the binding pocket were involved in constituting the van der Waals forces of attraction with various fragments of compound **S7**. The central triazine ring of **S4** was found to be engaged with the carboxylate anion of the Asp630 through π-anion force (2.70 Å), whereas Gly479, Glu520, and Arg635 were also forming π-anion forces (3.35, 3.54, 3.91, and 4.05 Å) with different aromatic rings of the ligand molecule. Two conventional hydrogen bonds were formed by one of the hydroxyl moieties with Glu551 (2.76 Å) and Ala553 (2.46 Å) amino acid residues, whereas amino acids Leu517 and Leu619 formed π–σ forces with the electronic clouds of aromatic rings of the ligand molecule. In the complex of compound **S6** with SRC protein, two conventional hydrogen bonds were formed by a nitrogen atom of triazine ring (2.05 Å) and a nitrogen atom of secondary amino group (3.08 Å) with Asn B:534 amino acid where the binding pocket to hold this ligand molecule was found to be at the interface of chains A and B of the target substrate. Further, the amino acid residues Asp1164, Ile1084, and Met1211 were important for constituting conventional hydrogen bond (2.76 Å) and π–σ forces (3.49, 3.83, and 3.97 Å), whereas a π–sulfur force (3.81 Å) was formed by the Met1211 amino acid residue. These strong binding interactions of various ligands with their target substrates hold them firmly in the binding pockets, which results in making them potent TKI candidates (Figures 6 and 7).

3.4. DFT Calculation Studies. Formal investigations were conducted to establish a connection between theoretical predictions and experimental observations of synthesized compounds **S1**−**S8**. The Gaussian 16 software was utilized for quantum chemistry calculations and geometrical optimization of each compound and GaussView 6.0.1 was used for visualization.[39,40]

The compounds were optimized by employing the B3LYP/6-31G(d) functional and basis, respectively. Following this, the methodology outlined earlier was applied to analyze Frontier molecular orbitals, nonlinear optical, natural bond orbitals, molecular electrostatic potential, and global reactivity descriptors of the synthesized compounds (**S1**−**S8**). The optimized structures for compounds **S1**−**S8** are shown in Figure 8.

3.4.1. Frontier Molecular Orbital (FMO) Analysis. The higher occupied molecular orbital (HOMO) and lower unoccupied molecular orbital (LUMO) jointly represent the two maximum critical molecular orbitals that determine a
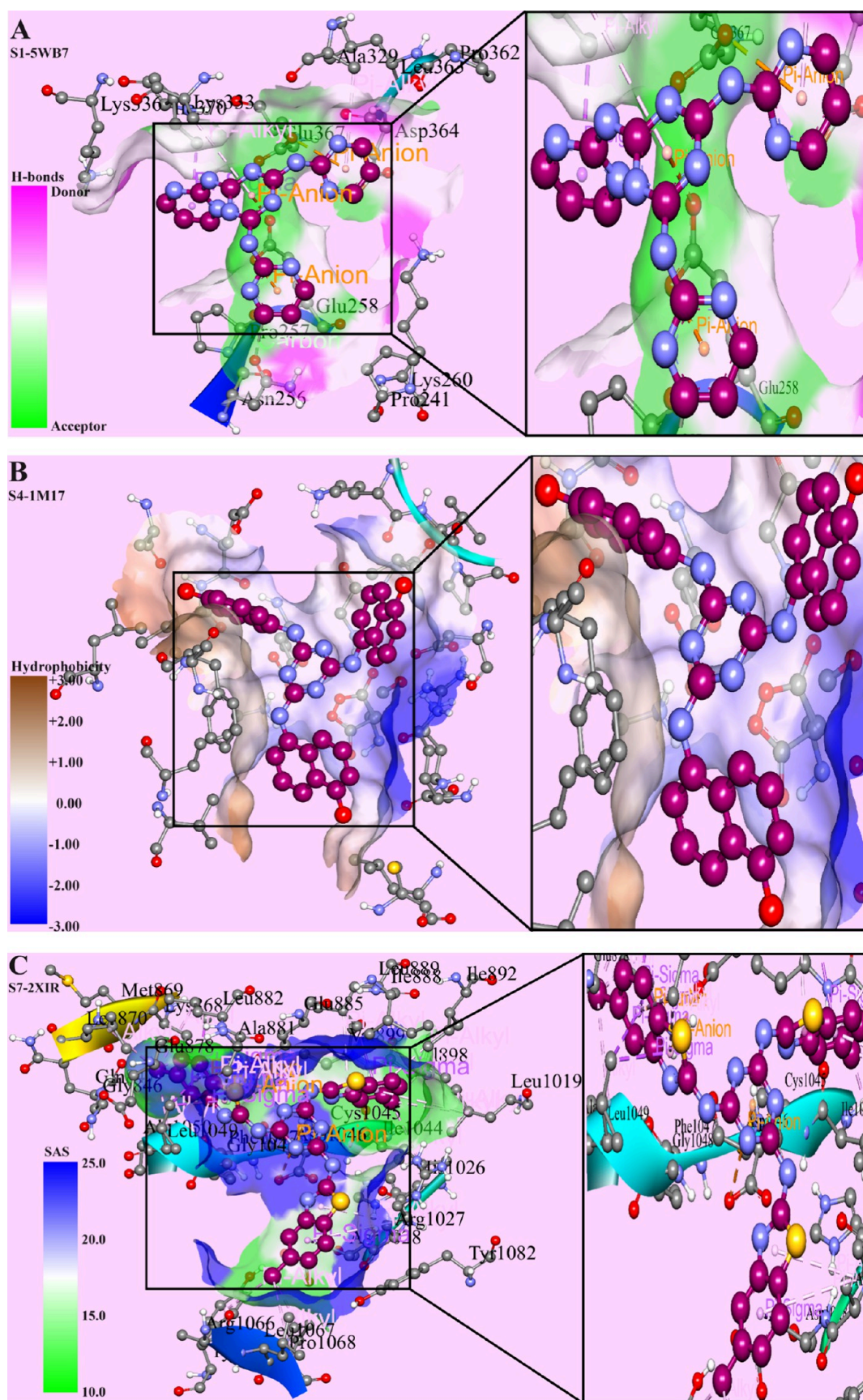
Figure 6. continued
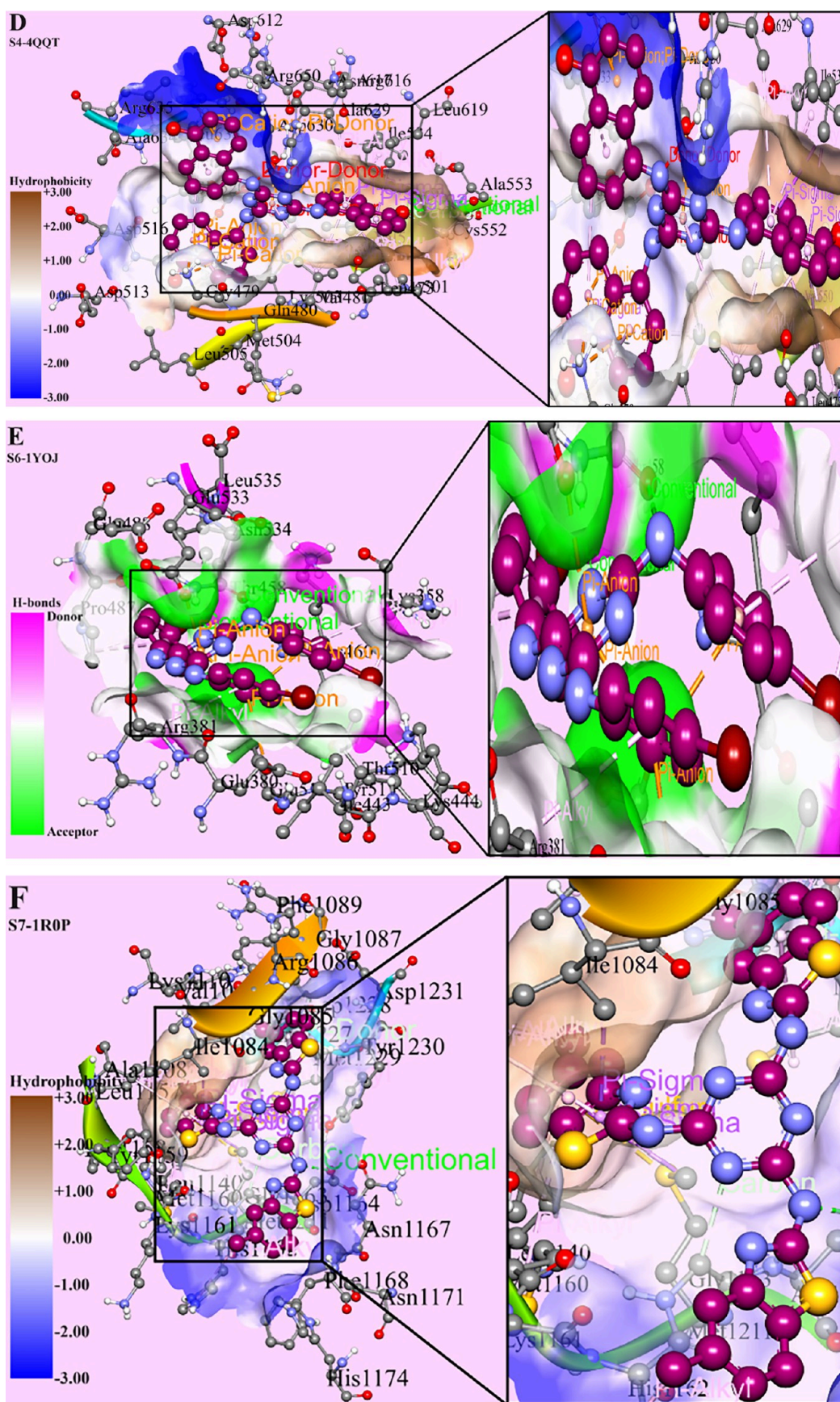
Figure 6. Three dimensional representations (A−F) of ligand−protein docked complexes of selected compounds with their target RTK proteins

Figure 7. 2D representations of ligand–protein interactions, H-bonding, and hydrophobic interactions of the selected compounds with amino acid residues in the binding pockets of their target RTK substrates.

molecule's chemical behavior, bioactivity, and physiological locations. These orbitals, sometimes referred to as the frontier molecular orbitals, are essential in understanding a molecule's

properties. The H−L energy gap, which represents the difference in energy between the HOMO and LUMO of a molecule, plays a significant role in determining the electronic

COMPOUNDS	OPTIMIZED STRUCTURES	CHEMDRAW STRUCTURES
S1		
S2		
S3		
S4		
S5		
S6		
S7		
S8		

Figure 8. Pictorial representation of the chemical structures, as well as the optimized geometries, of compounds **S1**−**S8**.

characteristics and reactivity of the molecule. A larger H−L energy gap is indicative of increased stability and lower reactivity, while a smaller H−L energy gap suggests increased

reactivity and lower stability. The energy gap, denoted by E_g, is a useful measure for evaluating the kinetic polarization, intramolecular charge transfer (ICT), and electronic spectra of a molecule.[41−43]

Table 5 exhibits the frontier molecular orbitals of **S1**−**S8**. The range of E_g for **S1**−**S8** is between 3.76 and 5.15 eV,

Table 5. E_{HOMO}, E_{LUMO}, and E_g of Molecules in eV

molecules	HOMO (eV)	LUMO (eV)	E_g (eV)
S1	−6.19	−1.03	5.15
S2	−5.42	−0.51	4.92
S3	−6.79	−2.63	4.16
S4	−5.34	−1.10	4.24
S5	−5.12	−0.38	4.74
S6	−5.85	−1.02	4.83
S7	−5.56	−1.81	3.76
S8	−6.43	−1.29	5.14

respectively. **S7**, **S4**, and **S3** are expected to exhibit increased reactivity due to their smaller energy gaps. Meanwhile, **S5**, **S2**, **S8**, and **S6** display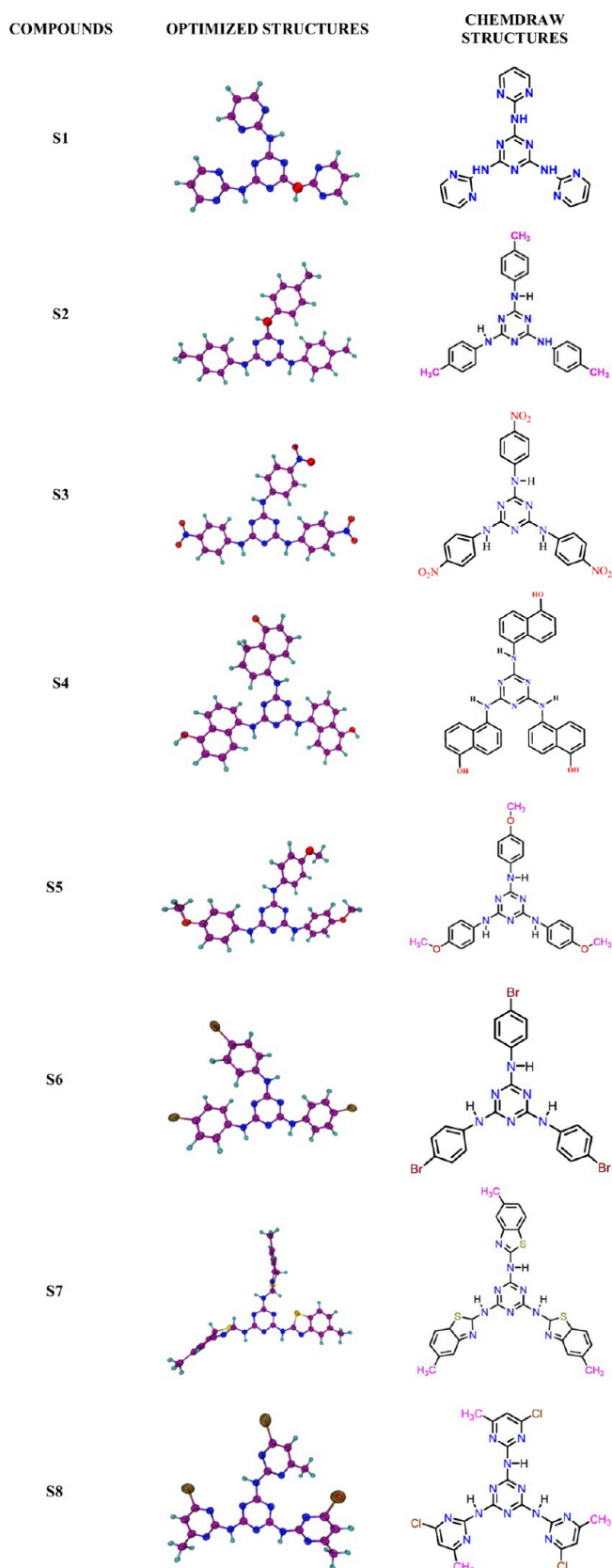 moderate reactivity, with slightly larger energy gaps. **S1**, on the other hand, is likely to possess reduced reactivity due to the largest energy gaps. The energy gaps offer a qualitative understanding of the electronic transitions within the compounds, revealing the energy necessary for transitions between distinct molecular orbitals. Smaller gaps typically suggest more accessible electronic transitions at lower energy levels, whereas larger gaps imply higher energy requirements and greater stability. Thus, **S7**, **S4**, and **S3**, with their smaller energy gaps, have relatively lower energy requirements for electronic transitions. Consequently, electronic transitions in these compounds are more likely to occur at lower energy levels. The frontier molecular orbitals of **S1**−**S8** are depicted in Figure 9.

3.4.2. Global Reactivity Descriptors. Global reactivity descriptors constitute a set of theoretical parameters employed in quantum chemistry and molecular modeling to evaluate the overall reactivity of a molecule. These descriptors comprise the electronegativity (X), electron affinity (A), electrophilicity (ω), chemical potential (μ), hardness (η), and softness (σ). The ionization potential represents the energy required to extract an electron from a neutral, isolated gaseous atom to form a cation. The electron affinity is the energy change associated with adding an electron to a neutral, isolated gaseous atom to form an anion. The electronegativity scale measures an atom's capacity to attract electrons in a chemical bond. These descriptors offer valuable insights into compounds' chemical reactivity and stability, enabling a deeper understanding of their behavior in chemical reactions and potential applications.

Table 6 illustrates the global reactivity descriptors of compounds **S1**−**S8**, which indicate that compounds **S3**, **S6**, **S7**, and **S8** generally exhibit higher values for the ionization potential, electron affinity, electronegativity, hardness, chemical potential, and global electrophilicity. These characteristics collectively suggest that these compounds are more stable, less likely to undergo electron loss, and have a stronger tendency to accept electrons, making them potentially less reactive. Table 6 also displays the values of the global nucleophilicity index ($\omega-$) and global dual descriptor ($\omega+$), which measure a compound's ability to donate electrons, making it a measure of nucleophilicity, and the compound's ability to both accept and donate electrons, indicating its dual nature, respectively. It
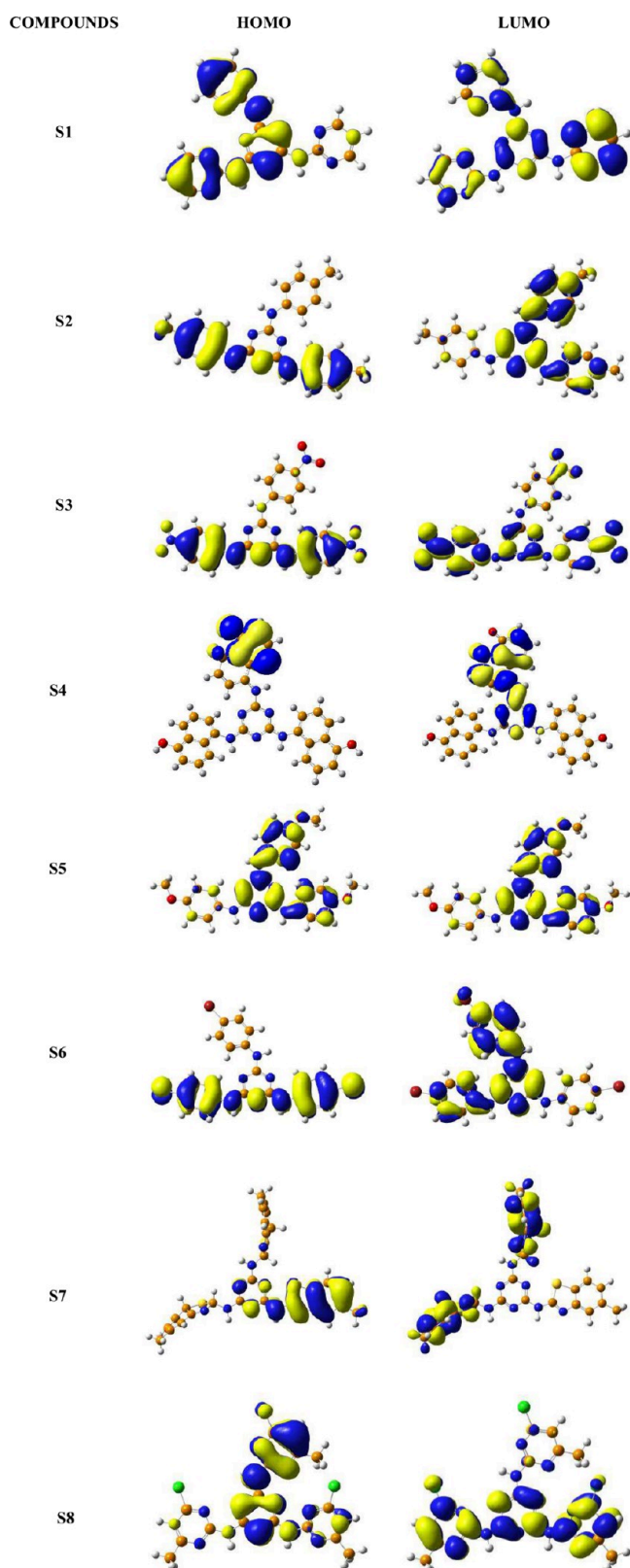
COMPOUNDS **HOMO** **LUMO**

S1

S2

S3

S4

S5

S6

S7

S8

Figure 9. HOMOs and LUMOs of compounds **S1–S8**.

appears that compounds **S3** and **S7** exhibit a stronger tendency toward nucleophilic and dual reactivity, while the other compounds exhibit a more balanced or electrophilic behavior.

3.4.3. Molecular Electrostatic Potential (MEP) Analysis. Molecular electrostatic potential maps are graphical represen-

tations that illustrate the distribution of charges within a compound in three-dimensional space. These maps enable researchers to visualize regions of varying charge densities within a compound and facilitate the evaluation of molecular interactions.

The analysis of the Molecular Electrostatic Potential (MEP) involves the assessment of three distinct molecular characteristics: electron-rich, electron-deficient, and neutral regions. In Figure 10, each MEP plot depicts three distinct color hues: red, blue, and green, which signify electron-rich, electron-deficient, and neutral regions, respectively. This analysis allows for a better understanding of the electrostatic interactions between different molecules based on their electrostatic potential profiles. Thus, the red region indicates a negatively charged and relatively weak electrostatic potential, while the blue region signifies a positively charged and strongly electrostatic potential. The blue region is indicative of a nucleophilic center, while the red region represents an electrophilic center.[44,45]

The electrostatic potential analysis of compounds **S1–S8** is illustrated in Figure 10. These compounds underwent a comprehensive 3D MEP analysis using the B3LYP/6-31G(d) functional. All of the compounds (**S1–S8**) exhibit a positively charged region (blue) that is aligned with the acceptor unit, while the corresponding donor unit displays a negatively charged region (red). A neutral electrostatic potential area is depicted in green.

3.4.4. Nonlinear Optical Analysis. The potential applications of nonlinear optical materials extend to a variety of fields, including optoelectronic devices, signal manipulation, and telecommunications. The effectiveness of donor–acceptor groups and their arrangement has a direct impact on the level of nonlinear optical efficiency.[46] To put it another way, nonlinear optical materials possess a conjugated structure with alternating electron-donating and electron-withdrawing elements, resulting from their π-electron-conjugated system and incorporating electron donor and acceptor groups at different terminals. This study has been expanded to evaluate the optical characteristics of compounds **S1–S8**, with the aim of their significant utilization in optoelectronics. The optoelectronic characteristics, including polarizability (α_{tot}), first-order hyperpolarizability (β_{tot}), and dipole moment (μ_{tot}), are calculated using the provided equation.

$$\mu_{tot} = (\mu_x^2 + \mu_y^2 + \mu_z^2)^{1/2}$$

$$\alpha_{tot} = \frac{1}{3}(\alpha_{xx} + \alpha_{yy} + \alpha_{zz})$$

$$\beta_{tot} = (\beta_x^2 + \beta_y^2 + \beta_z^2)^{1/2}$$

Table 7 presents the polarizability, hyperpolarizability, and dipole moment values of the compounds (**S1–S8**). The dipole moment quantifies the extent of positive and negative charge separation within a molecule, serving as an indicator of its overall polarity. The **S3** exhibits a notably high dipole moment, indicating a substantial charge separation and, consequently, a higher degree of polarity compared to the other compounds. In contrast, **S2** possesses a very low dipole moment, suggesting a weak separation of charges and implying that **S2** is likely to be less polar than the other compounds. Higher polarizability values indicate that an external electric field can easily distort a molecule. Increased electron cloud elasticity and responsiveness to an applied electric field may be related to this. The

Table 6. Computed Global Reactivity Descriptors for Compounds S1−S8

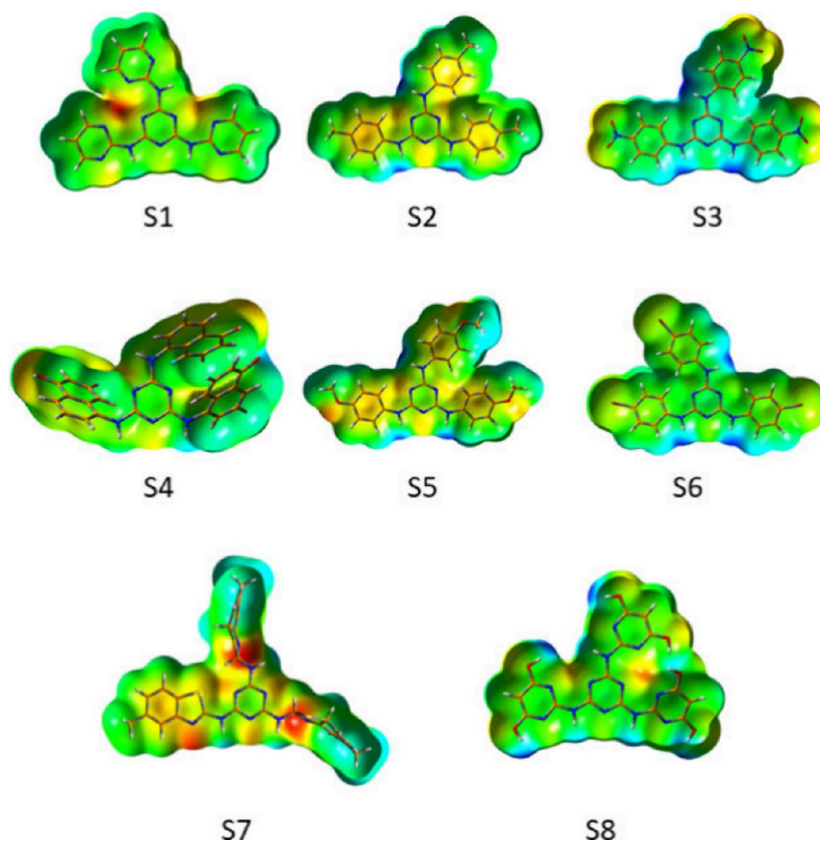| compounds	I	A	X	(η)	(μ)	Ω	$\omega-$	$\omega+$	S
S1	7.50	−0.20	3.65	3.85	−3.65	1.73	4.04	0.39	0.13
S2	6.64	−0.73	2.95	3.69	−2.95	1.18	3.12	0.17	0.14
S3	7.97	1.53	4.75	3.22	−4.75	3.50	6.27	1.53	0.16
S4	6.45	−0.02	3.22	3.23	−3.22	1.60	3.61	0.40	0.15
S5	6.30	−0.85	2.72	3.58	−2.72	1.04	2.85	0.12	0.14
S6	7.00	−0.19	3.41	3.59	−3.41	1.61	3.77	0.36	0.14
S7	6.87	0.67	3.77	3.10	−3.77	2.29	4.57	0.79	0.16
S8	7.93	−0.25	3.84	4.09	−3.84	1.80	4.23	0.39	0.12

Figure 10. Molecular electrostatic potential maps for compounds S1−S8.

Table 7. Polarizability, Hyperpolarizability (in au), and Dipole Moment (in Debye) of Compounds S1−S8

molecules	polarizability (α)	hyperpolarizability (β)	DM (μ)
S1	259.17	735.08	1.50
S2	333.56	855.64	0.29
S3	367.82	2866.69	6.86
S4	391.08	417.97	2.31
S5	348.33	771.23	1.77
S6	381.08	800.73	2.94
S7	449.34	1191.40	5.19
S8	336.94	527.24	5.30

polarizability values of S3 and S7 are comparatively higher, suggesting a stronger propensity for electronic deformation. A higher degree of nonlinear response to an external electric field is indicated by hyperpolarizability values. Higher β compound values are more effective at producing nonlinear optical effects. The hyperpolarizability values of S3 and S7 are higher, indicating their possible use in nonlinear optical applications.

Compounds S3 and S7 stand out with both higher polarizability and hyperpolarizability values, indicating their potential significance in applications where responsiveness to electric fields and nonlinear optical effects are crucial.

3.4.5. Natural Bond Orbital Analysis. Natural Bond Orbitals (NBO) constitute a computational methodology that has become indispensable for comprehending the intricate aspects of molecular electronic structures. Originally stemming from the domain of quantum chemistry, NBO serves as a tool for transforming intricate wave functions derived from electronic structure calculations into localized orbitals endowed with explicit chemical significance. The NBO methodology, grounded in second-order perturbation theory, systematically scrutinizes the electronic structure of a molecule. Through this approach, the NBO delineates a set of localized orbitals known as Natural Bond Orbitals, which align with specific chemical bonds or lone pairs. These localized orbitals offer a more lucid understanding of molecular bonding, facilitating the allocation of electron density to precise regions within the molecule.

The analysis of NBO involves the evaluation of various parameters, including second-order perturbation energy (E(2)), Fock matrix elements (F(i,j)), and energy differentials between donor and acceptor orbitals (E(j)-E(i)). Collectively, these parameters provide comprehensive insights into the strength, nature, and directional aspects of interactions within a molecular system.

The convergence of bonding and antibonding orbitals (C−C), (C−H), and (C−N) in **S1−S8** facilitates intermolecular hyper conjugative interactions, inducing intramolecular charge transfer (ICT) and ultimately stabilizing the molecular system. This phenomenon results in significant electron density, contributing to robust delocalization, as depicted in Table 8. Specifically, **S2**, **S7**, **S4**, and **S8** showcase robust $\pi-\pi$ interactions, yielding elevated E(2) values and substantial stabilization. Conversely, **S5** and **S6** exhibit moderate LP−π^* interactions, while **S3** demonstrates a compelling interaction involving a lone pair on oxygen and a π^* orbital. The notable E(2) values in these compounds signify pronounced stabilizing effects attributed to the aforementioned interactions.

4. CONCLUSION

This research project presents the synthesis of a small library of symmetrical trisubstituted triazine analogs using three different methodologies, namely, conventional, MW-assisted, and solid-supported MW-assisted synthesis using both organic and inorganic support. The synthesized compounds were tested against antibacterial and anticancer agents and were found to depict moderate to good activity, especially compounds containing pyrimidine, benzothiazole, or a phenyl ring substituted with NO_2, OH, and OCH_3. Moreover, the results of molecular docking studies performed against Receptor Tyrosine Kinases (RTKs) were also consistent with the *in vitro* anticancer activity, which depicted compounds **S3**, **S4**, **S6**, and **S7** to exhibit maximum potency and showed excellent binding energy values in the range of −7.14 to −13.30. Additionally, theoretical calculations regarding DFT studies such as FMO, MEP, and NLO, and various reactivity descriptors were also done.

The formation of these compounds using different methodologies was done to establish a comparative analysis in terms of yield, purity of the product, and the reaction time required. The results obtained indicated organic solid-supported MW-assisted methodology to be significantly better as compared to other synthetic techniques, as it not only fulfilled the norms of green chemistry, but also produced excellent yields of pure product within a short period. This was probably because of the interaction between the polymeric support and TCT that enhanced the reaction rate between substituted amines and the reagent cyanuric chloride. Also, no additional separation steps were required as workup, with cold water simply precipitated out the product, while the sulfonated polymer was separated during recrystallization. Thus, the MW-assisted organic polymer supported methodology is considered to be the best route for the synthesis of biologically active triazine scaffolds.

Table 8. Analysis of the Fock Matrix within the NBO Basis Using Second-Order Perturbation Theory for Compounds S1−S8

donor NBO (i)	acceptor NBO (j)	E(2) (kcal/mol)	E(j)-E(i) (a.u.)	F(i,j) (a.u.)
S1				
π^* C11−N21	π^* C19−C20	159.35	0.02	0.078
LP(1) N9	π^* C4−N5	57.1	0.26	0.111
LP(1) N23	σ^* C22−N27	12.98	0.87	0.096
σN3−C4	σ^* C2−N8	6.18	1.28	0.08
S2				
π^* C12−C18	π^* C21−C22	250.64	0.01	0.082
LP(1) N9	π^* C4−N5	62.75	0.25	0.116
LP(1) N5	σ^* N3−C4	12.87	0.85	0.095
σN8−H32	σ^* C2−N3	5.66	1.17	0.073
S3				
LP(3)O36	π^* N34−O35	162.39	0.14	0.138
πC4−N5	π^* N1−C6	41.33	0.3	0.105
LP(2) O29	σ^* N28−O30	19.28	0.7	0.105
σN3−C4	σ^* C2−N8	5.69	1.3	0.077
S4				
π^*C3−C4	π^* C5−C6	251.49	0.01	0.076
LP(1) N12	π^* C13−N15	55.26	0.26	0.112
πC5−C6	π^* C1−C2	26.28	0.27	0.075
σC27 - O30	LP*(1) H58	13.25	1.02	0.119
S5				
LP(1) N9	π^* C4−N5	62.84	0.25	0.117
πC4−N5	π^* N1−C6	41.46	0.3	0.106
LP(1) N5	σ^* N3−C4	12.84	0.85	0.095
σN8−H35	σ^* C2−N3	5.67	1.17	0.073
S6				
LP(1) N9	π^* C4−N5	63.02	0.25	0.117
πC4−N5	π^* N1−C6	41.96	0.3	0.106
LP(1) N1	σ^* N5−C6	13.78	0.91	0.101
σN3−C4	σ^* C2−N8	6.48	1.3	0.082
S7				
π^* C13−C18	π^* C14−C15	248.39	0.01	0.081
LP(1) N9	π^* C4−N5	66.49	0.24	0.119
LP(1) N1	σ^* N5−C6	13.17	0.87	0.097
σC11−N34	σ^* C33−C38	6.51	1.22	0.08
S8				
π^* N17−C18	π^* C11−N21	222.83	0.02	0.08
LP(1) N9	π^* C4−N5	56.56	0.25	0.11
LP(1) N21	σ^* C11−N17	14.37	0.83	0.099
σC11−N17	σ^* C18−Cl 30	6.1	0.96	0.069

■ ASSOCIATED CONTENT

ⓢ Supporting Information

The Supporting Information is available free of charge at https://pubs.acs.org/doi/10.1021/acsomega.4c01980.

Characterization: ^{1}H NMR spectra of the synthesized compounds; ^{13}C NMR spectra of the synthesized compounds; Mass spectra of the synthesized compounds; FTIR spectra of the synthesized compounds (PDF)

■ AUTHOR INFORMATION

Corresponding Authors

Sabir Ali Siddique − *Institute of Chemistry, The Islamia University of Bahawalpur, Bahawalpur 63100, Pakistan;* ⦿ orcid.org/0000-0002-2665-3080; Email: sabir.siddique@iub.edu.pk

Shahnaz − *Department of Chemistry, Lahore College for Women University, Lahore 44444, Pakistan;* Email: shahnazhej@gmail.com

Authors

Wajiha Akbar — *Department of Chemistry, Lahore College for Women University, Lahore 44444, Pakistan*

Shahana Ehsan — *Department of Chemistry, Lahore College for Women University, Lahore 44444, Pakistan*

Muhammad Sarfraz — *Institute of Chemistry, The Islamia University of Bahawalpur, Bahawalpur 63100, Pakistan*

Faiqa Shaheen — *School of Chemistry, University of the Punjab, Lahore 54590, Pakistan;* orcid.org/0000-0002-0879-5544

Ayesha Shafqat — *School of Botany, Minhaj University, Lahore 54770, Pakistan*

Muhammad Bilal Ahmed Siddique — *School of Chemistry and Chemical Engineering, Shandong University, Jinan 250100, People's Republic of China;* orcid.org/0000-0001-7005-1573

Ayesha Saeed — *Department of Chemistry, Lahore College for Women University, Lahore 44444, Pakistan*

Rashad Al-Salahi — *Department of Pharmaceutical Chemistry, College of Pharmacy, King Saud University, Riyadh 11451, Saudi Arabia;* orcid.org/0000-0003-1747-2736

Youness El Bakri — *Department of Theoretical and Applied Chemistry, South Ural State University, Chelyabinsk 454080, Russian Federation;* orcid.org/0000-0002-5759-6568

Complete contact information is available at:
https://pubs.acs.org/10.1021/acsomega.4c01980

Notes

The authors declare no competing financial interest.

■ REFERENCES

(1) Srinivas, K.; Srinivas, U.; Bhanuprakash, K.; Harakishore, K.; Murthy, U.S.N.; Jayathirtha Rao, V. Synthesis and antibacterial activity of various substituted s-triazines. *Eur. J. Med. Chem.* **2006**, *41*, 1240−1246.

(2) Patel, R. V.; Kumari, P.; Rajani, P. D.; Chikhalia, K. H. Synthesis and studies of novel 2-(4-cyano-3-trifluoromethylphenyl amino)-4-(quinoline-4-yloxy)-6-(piperazinyl/piperidinyl)-s-triazines as potential antimicrobial, antimycobacterial and anticancer agents. *Eur. J. Med. Chem.* **2011**, *46*, 4354−4365.

(3) Agrahari, B.; Layek, S.; Ganguly, R.; Dege, N.; Pathak, D. D. Synthesis, characterization and single crystal X-ray studies of pincer type Ni(II)-Schiff base complexes: Application in synthesis of 2-substituted benzimidazoles. *J. Organomet. Chem.* **2019**, *890*, 13−20.

(4) Cascioferro, S.; Parrino, B.; Spano, V.; Carbone, A.; Montalbano, A.; Barraja, P.; Diana, P.; Cirrincione, G. Synthesis and antitumor activities of 1,2,3-triazines and their benzo and heterofused derivatives. *Eur. J. Med. Chem.* **2017**, *142*, 74−86.

(5) Singla, P.; Luxami, V.; Paul, K. Triazine as a promising scaffold for its versatile biological behavior. *Eur. J. Med. Chem.* **2015**, *102*, 39−57.

(6) Cascioferro, S.; Parrino, B.; Spano, V.; Carbone, A.; Montalbano, A.; Barraja, P.; Diana, P.; Cirrincione, G. 1,3,5-Triazines: A promising scaffold for anticancer drugs development. *Eur. J. Med. Chem.* **2017**, *142*, 523−549.

(7) Jameel, E.; Meena, P.; Maqbool, M.; Kumar, J.; Ahmed, W.; Mumtazuddin, S.; Tiwari, M.; Hoda, N.; Jayaram, B. Rational design, synthesis and biological screening of triazine triazolopyrimidine hybrids as multitarget anti-Alzheimer agents. *Eur. J. Med. Chem.* **2017**, *136*, 36−51.

(8) Kumar, R.; Kumar, N.; Roy, R. K.; Singh, A. Triazines − A comprehensive review of their synthesis and diverse biological importance. *Curr. Med. Drug. Res.* **2017**, *1*, 1−12.

(9) Matulaitis, T.; Kostiv, N.; Grazulevicius, J. V.; Peciulyte, L.; Simokaitiene, J.; Jankauskas, V.; Luszczynska, B.; Ulanski, J. Synthesis and properties of bipolar derivatives of 1,3,5-triazine and carbazole. *Dyes Pigm.* **2016**, *127*, 45−58.

(10) Bartholomew, D. *Comprehensive Heterocyclic Chemistry II, Reference module in chemistry, molecular sciences and chemical engineering* **1996**, *6*, 575−636.

(11) Funfuenha, W.; Phakhodee, W.; Pattarawarapan, M. Facile and efficient synthesis of C2-symmetrical 1,3,5-triazine polycarboxylate ligands under microwave irradiation. *Tetrahedron* **2014**, *70*, 5415−5419.

(12) Maqbool, M.; Manral, A.; Jameel, E.; Kumar, J.; Saini, V.; Shandilya, A.; Tiwari, M.; Hoda, N.; Jayaram, B. Development of cyanopyridine−triazine hybrids as lead multitarget anti-Alzheimer agents. *Bioorg. Med. Chem.* **2016**, *24*, 2777−2788.

(13) Narva, S.; Chitti, S.; Amaroju, S.; Bhattacharjee, D.; Rao, B. B.; Jain, N.; Alvala, M.; Sekhar, K. V. G. C. Design and synthesis of 4-morpholino-6-(1,2,3,6-tetrahydropyridin4-yl)-N-(3,4,5-trimethoxy-phenyl)-1,3,5-triazin-2-amine analogues as tubulin polymerization inhibitors. *Bioorg. Med. Chem. Lett.* **2017**, *27*, 3794−3801.

(14) Chen, H.; Dao, P.; Laporte, A.; Garbay, C. High yielding microwave-assisted synthesis of 2-(arylmethyl)amino-4- arylamino-6-alkyl-1,3,5-triazines. *Tetrahedron Lett.* **2010**, *51*, 3174−3176.

(15) Ehsan, S.; Akbar, W.; Faisal, S.; Khan, B. Comparative analysis of solvent free, KHSO$_4$ and Ce(SO$_4$)$_2$ catalyzed microwave-assisted synthesis of 1, 3-diazacyclopenta-2, 4-dienes and evaluation of its antibacterial activity. *Pak. J. Sci.* **2018**, *70*, 56−62.

(16) Ehsan, S.; Rafiq, F.; Khan, B.; Akbar, W.; Faisal, S. Synthesis and Characterization of N-substituted pyrimidin-2-one carbohydrazide Derivatives via Microwave-Assisted Approach. *J. Chem. Soc. Pak.* **2018**, *40*, 536−542.

(17) Sagheer, T.; Ehsan, S.; Akbar, W.; Faisal, S. Solid-supported synthesis of n-alkylated derivatives of 5-bromopyrimidine-2,4-dione and study of their cytotoxic effect. *J. Chem. Soc. Pak.* **2018**, *40*, 742−748.

(18) Lee, C.-H.; Jin, G. F.; Yoon, J. H.; Jung, Y. J.; Lee, J.-D.; Cho, S.; Nakamura, H.; Kang, S. O. Synthesis and characterization of polar functional group substituted mono- and bis-(o-carboranyl)-1,3,5-triazine derivatives. *Tetrahedron Lett.* **2008**, *49*, 159−164.

(19) Ghasemi, M.; Turnbull, T.; Sebastian, S.; Kempson, I. The MTT Assay: Utility, Limitations, Pitfalls, and Interpretation in Bulk and Single-Cell Analysis. *Int. J. Mol. Sci.* **2021**, *22*, 12827.

(20) Sobierajska, E.; Konopka, M.; Janaszewska, A.; Piorecka, K.; Blauz, A.; Klajnert-Maculewicz, B.; Stanczyk, M.; Stanczyk, W. Unusual Enhancement of Doxorubicin Activity on Co-Delivery with Polyhedral Oligomeric Silsesquioxane (POSS). *Materials* **2017**, *10* (10), 559.

(21) Farooq, M.; Sharma, A.; Almarhoon, Z.; Al-Dhfyan, A.; El-Faham, A.; Taha, N. A.; Wadaan, M. A.M.; Torre, B. G.; Albericio, F. Design and synthesis of mono-and di-pyrazolyl-s-triazine derivatives, their anticancer profile in human cancer cell lines, and in vivo toxicity in zebrafish embryos. *Bioorg. Chem.* **2019**, *87*, 457−46.

(22) Wani, M. Y.; Bhat, A. R.; Azam, A.; Choi, I.; Athar, F. Probing the antiamoebic and cytotoxicity potency of novel tetrazole and triazine derivatives. *Eur. J. Med. Chem.* **2012**, *48*, 313−320.

(23) Łazewska, D.; Kurczab, R.ł; Wiecek, M.ł; Kaminska, K.; Satała, G.; Jastrzebska-Wiesek, M.; Partyka, A.; Bojarski, A. J.;

Wesołowska, A.; Kiec-Kononowicz, K.; Handzlik, J. The computer-aided discovery of novel family of the 5-HT6 serotonin receptor ligands among derivatives of 4-benzyl-1,3,5-triazine. *Eur. J. of. Med. Chem.* **2017**, *135* (28), 117−124.

(24) Sanner, M. F. Python: a programming language for software integration and development. *J. Mol. Graph Model* **1999**, *17* (1), 57−61.

(25) Berman, H. M.; Westbrook, J.; Feng, Z.; Gilliland, G.; Bhat, T. N.; Weissig, H.; Shindyalov, I. N.; Bourne, P. E. The protein data bank. *Nucleic acids research* **2000**, *28* (1), 235−242.

(26) O'Boyle, N. M.; Banck, M.; James, C. A.; Morley, C.; Vandermeersch, T.; Hutchison, G. R. Open Babel: An open chemical toolbox. *Journal of cheminformatics* **2011**, *3*, 1−14.

(27) Pottier, C.; Fresnais, M.; Gilon, M.; Jérusalem, G.; Longuespée, R.; Sounni, N. E. Tyrosine kinase inhibitors in cancer: breakthrough and challenges of targeted therapy. *Cancers* **2020**, *12* (3), 731.

(28) Ebrahimi, N.; Fardi, E.; Ghaderi, H.; Palizdar, S.; Khorram, R.; Vafadar, R.; Ghanaatian, M.; Rezaei-Tazangi, F.; Baziyar, P.; Ahmadi, A.; Hamblin, M. R.; Aref, A. R. Receptor tyrosine kinase inhibitors in cancer. *Cell. Mol. Life Sci.* **2023**, *80* (4), 104.

(29) Huang, M. Y.; Jiang, X. M.; Wang, B. L.; Sun, Y.; Lu, J. J. Combination therapy with PD-1/PD-L1 blockade in non-small cell lung cancer: strategies and mechanisms. *Pharmacology & therapeutics* **2021**, *219*, No. 107694.

(30) Zhong, L.; Li, Y.; Xiong, L.; Wang, W.; Wu, M.; Yuan, T.; Yang, W.; Tian, C.; Miao, Z.; Wang, T.; Yang, S. Small molecules in targeted cancer therapy: advances, challenges, and future perspectives. *Signal transduction and targeted therapy* **2021**, *6* (1), 1−48.

(31) Puccini, A.; Marín-Ramos, N. I.; Bergamo, F.; Schirripa, M.; Lonardi, S.; Lenz, H. J.; Loupakis, F.; Battaglin, F. Safety and Tolerability of c-MET Inhibitors in Cancer. *Drug Saf.* **2019**, *42* (2), 211−233.

(32) Kaufman, N. E.; Dhingra, S.; Jois, S. D.; Vicente, M. D. G. H. Molecular targeting of epidermal growth factor receptor (EGFR) and vascular endothelial growth factor receptor (VEGFR). *Molecules* **2021**, *26* (4), 1076.

(33) Sierra, J. R.; Cepero, V.; Giordano, S. Molecular mechanisms of acquired resistance to tyrosine kinase targeted therapy. *Mol. Cancer* **2010**, *9*, 75.

(34) Geoghegan, C.; Burgoyne, R.; Green, E.; Ball, E. An exploratory study to examine differences in adverse drug reactions experienced by male and female patients taking tyrosine kinase inhibitors at a tertiary cancer centre. *Journal of Oncology Pharmacy Practice* **2023**, *29*.

(35) Hussain, S.; Hussain, S.; Zafar, M. N.; Hussain, I.; Khan, F.; Mughal, E. U.; Tahir, M. N. Preliminary anticancer evaluation of new Pd (II) complexes bearing NNO donor ligands. Saudi. *Pharmaceutical Journal* **2024**, *32* (1), No. 101915.

(36) Sarfraz, M.; Rauf, A.; Keller, P.; Qureshi, A. M. N, N'-dialkyl-2-thiobarbituric acid based sulfonamides as potential SARS-CoV-2 main protease inhibitors. *Can. J. Chem.* **2021**, *99* (3), 330−345.

(37) Khair-ul-Bariyah, S.; Sarfraz, M.; Sharif, A.; Farooqi, Z. H.; Arshad, M.; Ahmed, E.; Ashraf, M.; Abdullah, S.; Arshad, M. N.; Waseem, A. Novel benzothiazole sulfonamides as potent α-glucosidase and cholinesterase inhibitors: Design, synthesis, structural properties, biological evaluation and docking studies. *J. Mol. Struct.* **2024**, *1299*, No. 137118.

(38) Siddique, S.; Hussain, K.; Shehzadi, N.; Arshad, M.; Arshad, M. N.; Iftikhar, S.; Saghir, F.; Shaukat, A.; Sarfraz, M.; Ahmed, N. Design, synthesis, biological evaluation and molecular docking studies of quinoline-anthranilic acid hybrids as potent anti-inflammatory drugs. *Organic & Biomolecular Chemistry* **2024**, *22* (18), 3708−3724.

(39) Frisch, M. J.; Trucks, G. W.; Schlegel, H. B.; Scuseria, G. E.; Robb, M. A.; Cheeseman, J. R.; Scalmani, G.; Barone, V.; Petersson, G. A.; Nakatsuji, H. *Gaussian 16*; Gaussian Inc., Wallingford, CT. 2016.

(40) Dennington, R.; Keith, T. A.; Millam, J. M. *GaussView 6.1.1.*, Semichem Inc., Shawnee Mission, KS, U.S.A., 2016.

(41) Jumabaev, A.; Holikulov, U.; Hushvaktov, H.; Issaoui, N.; Absanov, A. Intermolecular interactions in ethanol solution of OABA: Raman, Ftir, DFT, M062X, MEP, NBO, FMO, AIM, NCI, RDG analysis. *J. Mol. Liq.* **2023**, *377*, 121552.

(42) Sarfraz, M.; Ayyaz, M.; Rauf, A.; Yaqoob, A.; Tooba; Arif Ali, M.; Siddique, S. A.; Qureshi, A. M.; Sarfraz, M. H.; Aljowaie, R. M.; Almutairi, S. M.; Arshad, M. New Pyrimidinone Bearing Amino-methylenes and Schiff Bases as Potent Antioxidant, Antibacterial, SARS-CoV-2, and COVID-19 Main Protease M^{Pro} Inhibitors: Design, Synthesis, Bioactivities, and Computational Studies. *ACS Omega* **2024**, *9*, 25730−25747.

(43) Ayyaz, M.; Sarfraz, M.; Arshad, M.; Yaqoob, A.; Siddique, S. A.; Hussain, S.; Ali, M. A.; Qureshi, A. M.; Rauf, A. Design, synthesis, in-vitro biological screening and in-silico studies of 2-thioxodihydropyrimidinone based new aminomethylene scaffolds. *J. Mol. Struct.* **2024**, *1299*, No. 137153.

(44) El Bakri, Y.; Musrat Kurbanova, M.; Ali Siddique, S.; Ahmad, S.; Goumri-Said, S. one-pot synthesis, X-ray structure, and identification of potential molecules against COVID-19 main protease through structure-guided and simulation approach. *Arab. J. Chem.* **2022**, *15*, 104230.

(45) Ahmed, K.; Bashir, M.; Bano, R.; Sarfraz, M.; Khan, H. U.; Khan, S.; Sharif, A.; Waseem, A.; Gilani, M. A.; Batool, K.; Idrees, R.; Rauf, A.; Saleem, R. S. Z.; Arshad, M. Potent heteroaromatic hydrazone based 1, 2, 4-triazine motifs: synthesis, anti-oxidant activity, cholinesterase inhibition, quantum chemical and molecular docking studies. *J. Mol. Struct.* **2023**, *1284*, No. 135383.

(46) Kurtz, H. A.; Stewart, J. J. P.; Dieter, K. M. Calculation of the nonlinear optical properties of molecules. *J. Comput. Chem.* **1990**, *11*, 82−87.